LETTER Communicated by Idan Segev

Dynamic Moment Analysis of the Extracellular Electric Field of a Biologically Realistic Spiking Neuron

Joshua N. Milstein
milstein@caltech.edu
Christof Koch
koch@klab.caltech.edu
California Institute of Technology, Pasadena, CA 91125, U.S.A.

Based on the membrane currents generated by an action potential in a biologically realistic model of a pyramidal, hippocampal cell within rat CA1, we perform a moment expansion of the extracellular field potential. We decompose the potential into both inverse and classical moments and show that this method is a rapid and efficient way to calculate the extracellular field both near and far from the cell body. The action potential gives rise to a large quadrupole moment that contributes to the extracellular field up to distances of almost 1 cm. This method will serve as a starting point in connecting the microscopic generation of electric fields at the level of neurons to macroscopic observables such as the local field potential.

1 Introduction

Since the pioneering work of Hodgkin and Huxley in the early fifties (Hodgkin & Huxley, 1952) on the initiation and propagation of action potentials within the squid giant axon, there has been significant progress in our understanding of brain function at the level of the single neuron (Koch, 1999). Unfortunately, it has proved difficult to connect function at this microscopic scale to more global, large-scale brain function. In this letter, we work toward this goal by developing a physiologically accurate model of the extracellular field of a single neuron, which may be efficiently employed to model the field associated with very large numbers of neurons.

The dominant means of rapid communication among neurons is through chemically or electrically mediated synapses. Ephatic interactions, where communication is directly via an electric field, may occur in nerves that have been crushed or damaged by neurodegenerative disorders such as multiple sclerosis (Faber & Korn, 1989; Jefferys, 1995), but examples of ephatic effects under normal conditions are rare (Korn & Axelrad, 1980; Korn & Faber, 1980). Nonetheless, all electronic, cellular activity generates extracellular electric fields, and so it is natural to ask if these fields have

any relevance to the functioning of the brain. Before we can begin to answer this question, however, we need to consider how best to model these fields.

Our current objective is to better understand the forward problem of modeling the extracellular field of various regions of the brain from the underlying neural activity and to develop an accurate and efficient method for modeling these fields. A full construction of the extracellular field, from single-neuron activity, is extremely difficult. For instance, to generate microvolt potentials, as commonly detected by electroencephalograph (EEG) scalp recordings, requires the superposition of activity from a great number of neurons. A simple estimate is that it takes a 6 cm^2 patch of cortical tissue, containing around 6×10^7 synchronously active neurons, to generate a detectable signal on the order of microvolts (Ebersole, 1997). Nonetheless, the microscopic behavior, although too difficult to incorporate exactly, may act as a guide in developing more coarsely grained models (Srinivasan, 2006). For instance, field theories of thalamic and cortical activity, constrained by physiological parameters, have recently been developed and have proven successful in quantitatively reproducing various EEG phenomena, evoked response potentials, coherence functions, and seizure dynamics, among others (Jirsa & Haken, 1996; Robinson et al., 2001; Robinson, Rennie, Rowe, O'Conner, & Gordon, 2005).

Neurons display a variety of complicated geometries, giving rise to an array of current distributions that dynamically vary throughout the course of an action potential and during the interspike interval. For local probes of individual neurons—for instance, by microelectrodes—the field generated by the action potential dominates, particularly near the soma. However, it is thought that synaptic activity as well as longer-lasting depolarization and hyperpolarizations are mainly responsible for the electrical activity detected by EEG recordings (Nunez & Srinivasan, 2006). There are two primary reasons that the contribution of the action potential is thought to be negligible to the fields detected by EEGs. First, in general, the dendritic axes of pyramidal cells lie parallel to the cortical sheet, which allows the contribution of the extracellular fields of the dendrites to add constructively, whereas the relative orientations of their axons are more varied, leading to a significantly reduced axonal contribution. Second, due to the relatively brief time course of an action potential, neurons would need to precisely synchronize their firing in order to generate a significant contribution to the extracellular field.

In the study examined here, we focus on the extracellular field of a single spiking cell, with the future intention of quantifying hypotheses such as those discussed above on the importance of the action potential to the extracellular field. We base our work on a quantitatively accurate model of a pyramidal cell that our lab has developed and use this model to ask questions regarding the local extracellular field, for instance, the field generated by a single neuron or a minicolumn of pyramidal neurons, and

later address how our results are relevant to more distant, global recordings, such as EEGs.

The dynamics of the extracellular field of a spiking neuron are rather complex. One would like to remove some of the complexity of analyzing the extracellular field of realistic neurons by identifying the essential features that characterize the current distributions. With this intention, our approach is to perform a moment expansion about the current distribution of the cell and to study the resulting, dynamical moments. Moment expansions are routinely used in molecular biology to aid in the calculation of Coulomb-mediated molecular interactions where the full electrostatic charge density may be quite complicated. They have been used to clarify the possible interactions between normal and alkylated DNA base pairs (Price, Celso, Treichel, Goodfellow, & Umrania, 1993), to model ligand binding and protein-protein interactions (Neves-Petersen & Petersen, 2003), and to simulate charge transport in biological ion channels (Saraniti, Aboud, & Eilsenberg, 2006), to name only a few applications. Our goal is twofold: to show that the dynamical moments of a biologically realistic neuron can be efficiently calculated and then see what simplifying features emerge from such an analysis.

Our approach naturally leads to several fundamental questions that have not been sufficiently addressed: When is it justified to model the neuron by a dipole? Is there a region of interest where the first few moments provide a useful approximation to the extracellular field? Close to the cell, do any of the moments dominate, or must we account for the full complexity of the current distribution? We present a method that is able to accurately and efficiently decompose the extracellular field into its fundamental moments at all distances from the cell body. We then discuss the usefulness of such an approach in describing local and global extracellular fields generated by networks of neurons.

2 Generalized Multipole Expansion

We begin by writing an equation for the extracellular field of a continuous source of currents within the point-source approximation,

$$\phi(\mathbf{x}) = \frac{1}{4\pi\sigma} \int d^3x' \frac{i(\mathbf{x}')}{|\mathbf{x} - \mathbf{x}'|}, \tag{2.1}$$

where $i(\mathbf{x}')$ is the current at location $\mathbf{x}'$ and $\mathbf{x} - \mathbf{x}'$ defines a vector that points from the current source toward a test point at $\mathbf{x}$. We will assume that the extracellular medium may be approximated as a homogeneous, isotropic volume conductor, and therefore the bulk conductivity tensor σ, may be taken as a constant. For frequency ranges between roughly 1 and 3000 Hz, capacitive effects are negligible, and a purely ohmic conductivity is sufficient for modeling the extracellular milieu. The validity of this approximation

is discussed in detail in Holt and Koch (1999), Plonsey (1969), and Bedard, Kroger, and Destexthe (2004). Typical values of the bulk conductivity, range between 200 and 400 $\Omega \cdot$ cm.

Since we are interested in a multipole expansion of the cell's current distribution at all distances from the cell, we need to pay particular attention to the convergence properties of our expansion method. The usual decomposition into multipoles is based on the following expansion of the $1/|\mathbf{x} - \mathbf{x}'|$ dependence of the electric potential into radial components r and spherical harmonics $Y_{l,m}(\theta, \phi)$:

$$\frac{1}{|\mathbf{x} - \mathbf{x}'|} = \sum_{l=0}^{\infty} \sum_{m=-l}^{l} \frac{1}{2l+1} \frac{r_<^l}{r_>^{l+1}} Y_{l,m}^*(\theta', \varphi') Y_{l,m}(\theta, \varphi). \tag{2.2}$$

The symbol $r_<$ refers to the smaller of the two values of $|\mathbf{x}|$ and $|\mathbf{x}'|$ (e.g., $\mathbf{x}$ may be the vector that points to the test point while $\mathbf{x}'$ points to the current source), while $r_>$ refers to the greater value. This condition will ensure that the sum is convergent, so special care needs to be taken to abide by this criterion. The classical multipole expansion assumes that we are outside the range of the current distribution, so we may identify $r_<$ with the magnitude of the vector pointing at current source r', while $r_>$ is associated with a test point at r. However, due to the complicated geometry displayed by different neurons, we may easily find ourselves within a regime in which the identities of these two quantities are swapped.

Figure 1 clarifies this point. We divide the extracellular region of a stereotypical pyramidal cell into two distinct volumes. For convenience, we pick a point roughly halfway up the apical dendrite of the cell as our origin; however, this choice is arbitrary—for instance, we could have chosen the origin to fall within the soma. Our choice of origin simply minimizes the total spherical volume of the current-containing region, which will later aid in the numerics. For a test point at $\mathbf{r}$, the region R_1 denotes the volume over which $r_< = r', r_> = r$, while region R_2 is the volume where $r_< = r, r_> = r'$. The solid line separates these two regions. It is clear that for any value of $\mathbf{r}$ where there still exists an element of current outside the volume enclosed by that vector, we need to be careful that we have properly identified $r_<$ and $r_>$. This leads to a natural splitting of extracellular space into two regions, which is denoted by the dashed line in the figure. We will refer to a test point within the volume enclosed by the dashed line as in the inner field, while points outside will be considered the outer field. We employ this terminology since the regions we are considering are somewhat different from the more typically encountered "near" and "far" field. The important distinction between this definition of an inner and outer field is that the outer field defines the region in which $\{r_<, r_>\}$ are static, whereas within the inner field, $\{r_<, r_>\}$ vary based on the placement of the test point. For instance, for scalp recordings several centimeters from the relevant cells, one

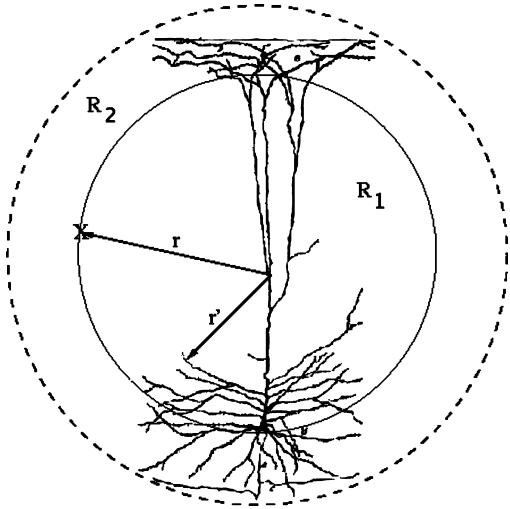

Figure 1: The various regions into which the generalized multipole expansion is divided. Vector **r'** points to the current source, while vector **r** is directed toward the test point. The solid circle divides region R_2 from R_1. The dashed line marks the divide between the inner (inside) and outer (outside) field regions. The pyramidal cell depicted is purely illustrative.

is within the outer field, but for intracranial recordings millimeters from a cortical microcolumn, one might have to account for the inner field based on the position of the electrode.

We may now write the following moment expansion of the extracellular potential:

$$\phi(\mathbf{x}) = \frac{1}{\sigma} \sum_{l=0}^{\infty} \sum_{m=-l}^{l} Y_{l,m}(\theta, \varphi) \left(\frac{q_{l,m}}{r^{l+1}} + r^l p_{l,m} \right), \tag{2.3}$$

where

$$q_{l,m} = \int_{R_1} d^3x' i(\mathbf{x}') r'^l Y^*_{l,m}(\theta', \varphi') \tag{2.4}$$

$$p_{l,m} = \int_{R_2} d^3x' \frac{i(\mathbf{x}')}{r'^{l+1}} Y^*_{l,m}(\theta', \varphi'). \tag{2.5}$$

Equations 2.4 and 2.5 are the moments of the potential, $q_{l,m}$ are the classical multipole moments, and $p_{l,m}$ are the less familiar inverse moments. If we write the elements of the multipole expansion as

$\phi_{l,m}(\mathbf{x}) = Y_{l,m}(\theta, \varphi)(\phi_{q_{l,m}}(r) + \phi_{p_{l,m}}(r))$, from equation 2.3, we may define the classical and inverse radial potentials:

$$\phi_{q_{l,m}}(r) \equiv \frac{1}{\sigma} \frac{q_{l,m}}{r^{l+1}} \quad \text{and} \quad \phi_{p_{l,m}}(r) \equiv \frac{1}{\sigma} p_{l,m} r^l, \tag{2.6}$$

respectively. The radial potentials will be helpful in comparing the relative importance of the moments in the multipole expansion. Note the radial dependencies in equation 2.3 that guarantee convergence of the expansion. In the outer field, this simply reduces to the standard multipole expansion, but the series remains convergent within the inner field as well as long as we restrict our integration over the appropriate volume elements as denoted in equations 2.4 and 2.5 and illustrated in Figure 1. A similar approach has recently been used to study the electrostatic potential of topological atoms, from which we have borrowed some of our terminology (Rafat & Popelier, 2005).

3 Model Cell

The cell that we will work with is a biologically realistic model of a hippocampal pyramidal cell within rat CA1. The model was developed in Gold, Henze, Koch, and Buzsaki (2006) to compare intracellular recordings to simultaneous extracellular recordings of neural activity. The active ionic currents were modeled using Hodgkin-Huxley-style kinetics. Voltage-dependent currents were carried by Na^+, K^+, and Ca^{2+} ions and were modeled for 12 different current processes. Details of the model can be found in Gold et al. (2006). To calculate the extracellular field, we first computed the transmembrane currents for the neuron along with their associated ionic currents. Standard 1D compartmental simulations where performed within the NEURON simulation environment (Hines & Carnevale, 1997). Approximately 1000 compartments where used to model an anatomically correct 3D reconstruction of the cell.

Within the first 1 ms of the simulation, we artificially depolarize the cell until an action potential is triggered within the soma; the cell dynamics follow the course of the action potential until the cell repolarizes and returns to a stable resting potential. This choice of initiating the action potential is arbitrary; we could likewise apply the procedure discussed here to a cell whose firing is initiated by synaptic input. Figure 2 shows the time course of the membrane current across a representative segment of the soma. Throughout, we assume that the extracellular potential is constant and equal to zero. We also assume that the transmembrane currents are not influenced by the evolving extracellular potentials ($\ll$ 1mV). An iterative procedure could be used to improve upon this approximation, although the modification can be shown to be negligible (Holt & Koch, 1999).

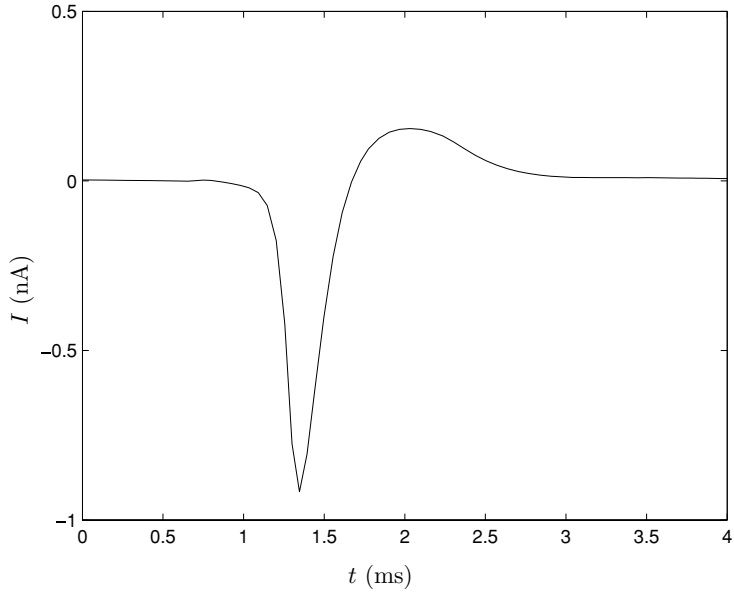

Figure 2: A representative time course of the total current across the soma showing the rapid inward (negative) Na^+ current, leading to the peak in the action potential and the slower, outward (positive) K^+ current that repolarizes the cell. Simulated synaptic input occurs within the first 1 ms triggering the firing of an action potential.

To study the moments that generate the extracellular field of a pyramidal cell, we take advantage of the fact that these cells are almost, but not quite, cylindrically symmetric (see Figure 3). As a first pass, we assume that any anisotropy coming from the branched structure of the dendrites is unimportant. Assuming cylindrical symmetry allows us to reduce the dimensionality of the system from a three-dimensional calculation to a problem of only two dimensions, but should modify only the quantitative, as opposed to qualitative, aspects of our results.

We first project the neuron on a plane parallel to the long axis of the cell body (see Figure 4a). For a cortical pyramidal cell, the view would correspond to having flattened out the cortex and then looking at the cell in the plane of the cortical sheet with the axon and basal dendrites toward the bottom and the apical and distal dendrites reaching upward. Each point in the figure corresponds to a current segment in the full, multicompartmental model of this cell. It is clear that the cell is not completely symmetric since the left and right portions, relative to the vertical axis of the cell, do not exactly correspond. However, we neglect this anisotropy and simply mirror the cell along this axis, averaging any overlapping current segments (see Figure 4b). After performing this simple transformation, we now assume

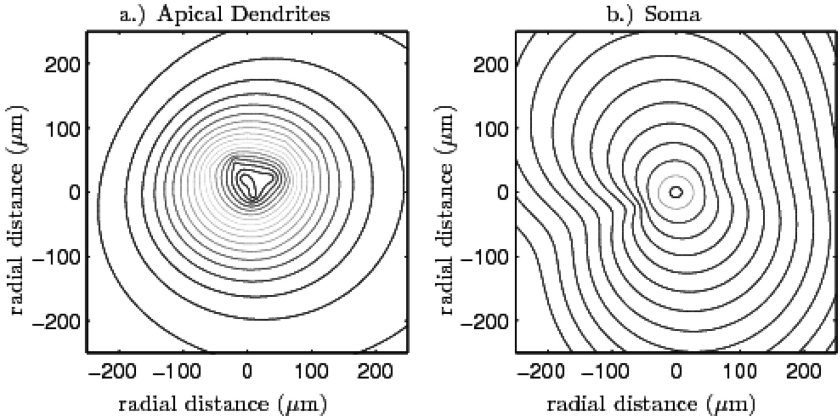

Figure 3: Equipotential curves taken at the peak of the action potential, calculated from the original pyramidal cell, illustrating the approximate cylindrical symmetry of the extracellular potential. We plot two cases above: (a) a plane at $z = 250\,\mu$m, within the apical dendrites and (b) a plane at $z = 0$, which is the location of the soma.

cylindrical symmetry along the vertical axis of the cell, with the current elements providing a current density over the corresponding cylindrical volume. Viewed out of plane, the cell would appear as an assortment of cylindrical annuli.

By symmetrizing the cell, we greatly simplify the problem, since all terms where $m \neq 0$ integrate to zero in equation 2.3. The remaining $m = 0$ spherical harmonics are related to the Laguerre polynomials, $P_l(x)$, via $Y_{l,0}(\theta, \varphi) = \sqrt{(2l+1)/(4\pi)}P_l(\cos\theta)$, which simplifies equation 2.3 and the calculation of the moments in equations 2.4 and 2.5.

4 Inner-Field Cellular Moments

We begin our analysis by considering the near-field moments that are relevant to local intracranial recordings of neural activity. In the inner field, because of the changing volumes of the regions defined by R_1 and R_2, both classical and inverse moments are dependent on distance. To efficiently compute the multipole expansion within this domain, we follow a similar procedure to that outlined in Rafat and Popelier (2005). The idea is to divide the inner field into a series of N spherical shells and then calculate the classical and inverse moments in a piecewise fashion within each shell. This calculation needs to be performed only once at each time step and may then be stored within a lookup table. To calculate the extracellular field of the cell requires the evaluation of the integrals in equations 2.4 and 2.5, which now become sums over the appropriate subset of N shells, with an interpolation

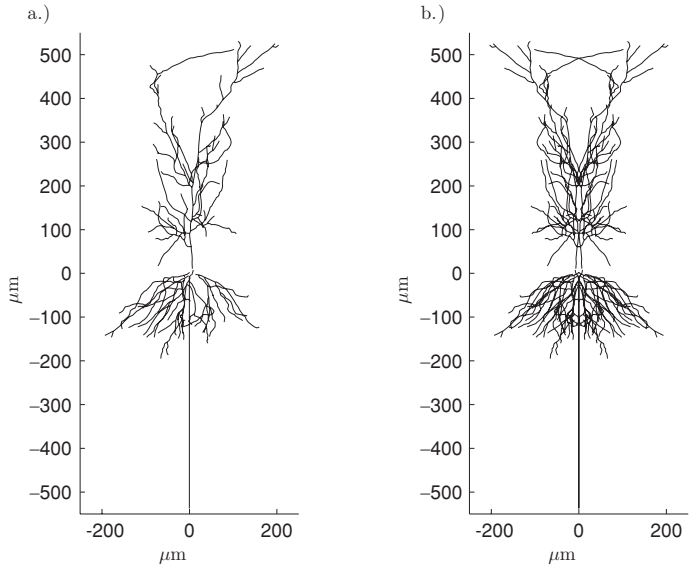

Figure 4: (a) A projection of the pyramidal neuron onto a plane perpendicular to the cortical section. (b) The original cell is symmetrized to simplify the analysis.

performed at the boundary between regions R_2 and R_1. Since the brunt of the numerics may be performed ahead of time and stored within computer memory, this method provides an efficient way of calculating the moments at any radial distance within the inner field granted that the expansion converges for a modest number of terms. For the model pyramidal cell that we investigate, as an example, we take $N = 200$ shells recorded over 200 time steps. To store the first 25 inverse and classical moments, we must generate a lookup table of approximately 16 Mb, which can easily be stored in the memory of a desktop computer.

One might hope that only the first few moments define the extracellular field of the cell; however, within the near field, the current distribution is too complex to allow such a simplification and the moment expansion contains many comparable terms throughout the time course of the action potential. We illustrate this in Figure 5 for a representative time ($t = 1.4$ ms, corresponding to the peak in the action potential) where, for clarity, we display only the first 11 classical $\phi_{q_l}(r)$ and 11 inverse $\phi_{p_l}(r)$ radial potentials.

The fairly slow convergence of the weights of the expansion, displayed in Figure 5, is similar for various times about the action potential. If we exclude a radius of 10 to 15 μm about the center of the cell, guaranteeing we are outside the body of the cell itself, the first 25 classical and inverse moments are needed to account for the total potential to within a few percent throughout the entire time course of the action potential.

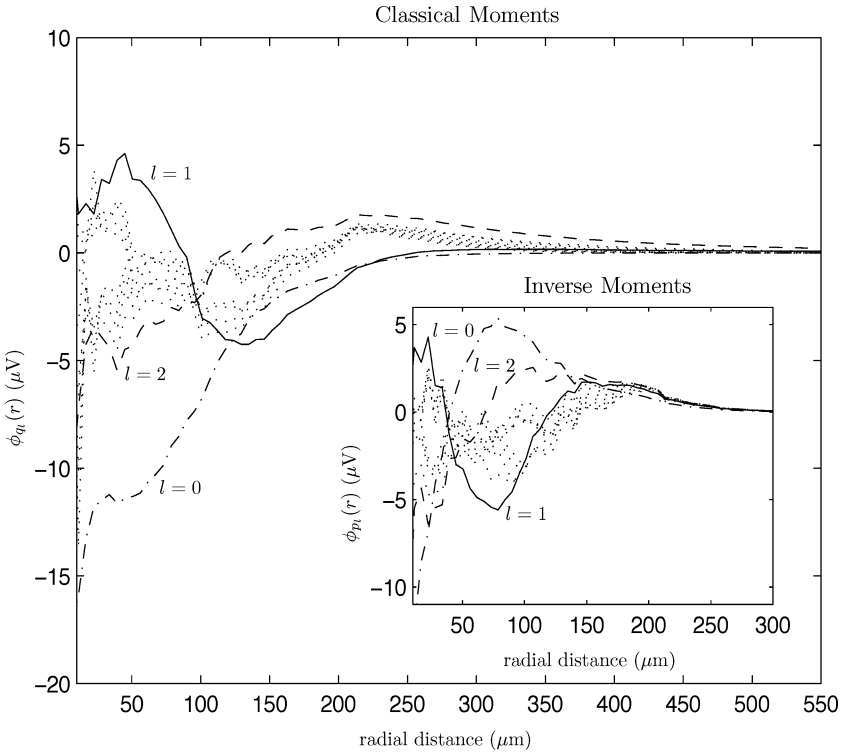

Figure 5: The radial potentials $\phi_q(r)$ for the first 11 classical moments as a function of radial distance at $t = 1.4$ ms, corresponding to the peak of the action potential. The $l = 0$ monopole moment (dash-dotted line), $l = 1$ dipole (solid line), and the $l = 2$ quadrupole (dashed line) are emphasized alongside the remaining moments up to $l = 10$ (dotted lines). Insert: The radial potential $\phi_p(r)$ for the first 11 inverse moments (same line labels as before) .

From Figure 5 it is hard to justify any dominant moments of the cellular current distribution due to the strong radial dependence displayed. This clearly implies that if we were to model the extracellular field of this neuron within radial distances on the order of half the length of the cell (about 550 μm), we must account for the full complexity of the current distribution, and that any assumption of treating such a complex current distribution as, perhaps an oscillating dipole, would be unjustified. Nonetheless, summing over roughly 50 elements (25 inverse moments and 25 classical moments) is a much quicker way to evaluate the extracellular field than summing over the 1000 or so current sources of the compartmental model. We next turn our attention to the outer-field results.

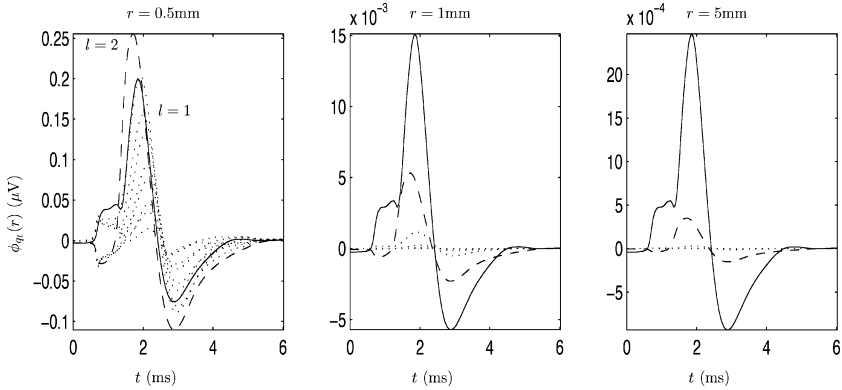

Figure 6: The radial potential $\phi_q(r)$ from the first 11 classical moments, as a function of time, at various distances from the cell origin. The $l = 1$ dipole moment (solid line) and the $l = 2$ quadrupole moment (dashed line) are emphasized. For comparison, the higher moments (dotted lines), up to $l = 10$, are shown.

5 Outer-Field Cellular Moments

Within the outer field, our problem simplifies to a moment calculation that can be performed without any of the complexities introduced within the inner field. One might assume, since the total current across the single neuron is conserved (i.e., the $l = 0$ moment is zero), that far from the cell, the only significant contributions would come from the dipole moment ($l = 1$). However, the quadrupole moment scales only one inverse power of r faster ($1/r^3$ as compared to $1/r^2$). If we compare the magnitude of the $1/r^2$ dipole potential to the $1/r^3$ quadrupole potential at a point on the boundary between the inner and outer field ($r \sim 0.5$ mm, which is half the length of the cell), in order for the quadrupole component to remain at, say, 10% of the magnitude of the dipole component after a distance of about 1 cm, ignoring angular dependencies, the initial magnitude of the quadrupole term at the boundary needs to be only on the order of twice as large as the dipole term at that same point. This means that if the magnitude of the quadrupole moment ever exceeds that of the dipole moment at the boundary to the outer field, there may be a significant region in which the quadrupole moment cannot be neglected.

We stress the above point because our numerical results for the model pyramidal cell we have been considering display a rather large quadrupole moment at various times during the action potential. Figure 6 shows the contribution of the first 11 classical moments, over the course of the action potential, as we progressively move away from the cell. At the cell boundary ($r \sim 0.5$ mm), the quadrupole is seen to surpass the dipole moment throughout most of the time course, whereas the higher-order moments

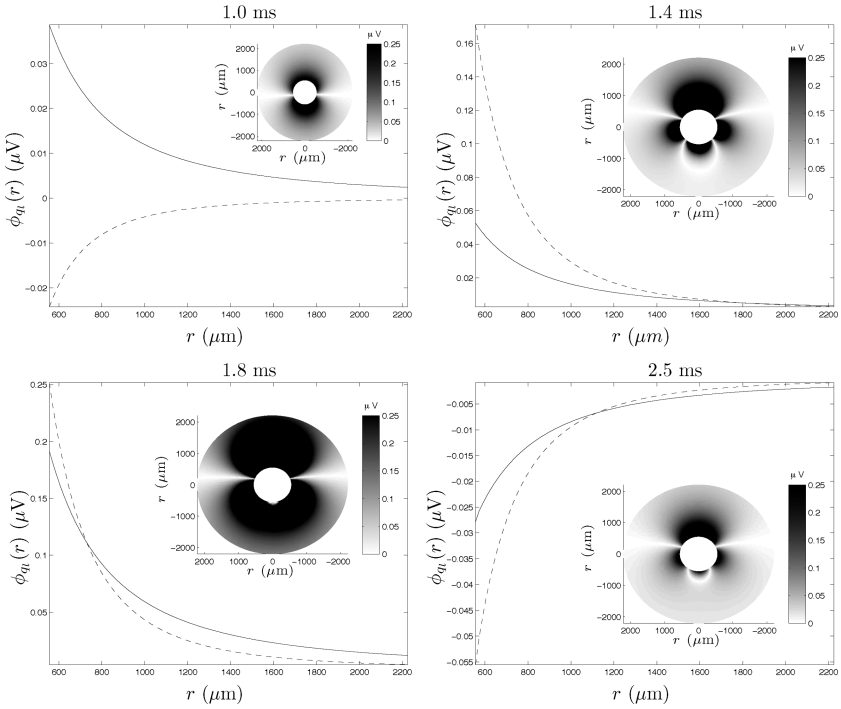

Figure 7: Moment comparison in the outer field, about the peak in the action potential. The main figures show only the dominant dipole $l = 1$ (solid line) and quadrupole $l = 2$ (dashed line) contributions to the radial potential $\phi_q(r)$. The insets show the absolute value of the resulting total potential in μV. Excluded is the inner field ($r < 550\,\mu$m) where the cell would be oriented along its vertical axis, as shown in Figure 4. Left to right, starting on the top, the times are given by 1.0, 1.4, 1.8, and 2.5 ms.

progressively decay. At a radial distance of roughly 1 mm, the quadrupole is clearly displayed while the higher moments are quickly decaying, and at a distance of $r \sim 0.5$ cm, only the dipole and quadrupole remain, with a significant contribution from the quadrupole.

Figure 7 displays the radial contribution to the extracellular potential from the dipole and quadrupole moment. (High-resolution color images and animations of the extracellular potentials can be found online at http://www.klab.caltech.edu/~milstein/moments.) As previously shown, these two moments dominate the extracellular field in the outer field throughout the action potential, except at points close to the boundary. We therefore neglect the contributions of all higher moments ($l > 2$) in the figures. At approximately 1 ms into the simulation, the cell begins to spike, and a large dipole moment dominates. However, as the action

potential grows, a significant quadrupole moment emerges. The initial magnitude of this moment is more than three times that of the dipole, which means that it will contribute to the extracellular field over a significant spatial extent. When the action potential has peaked, the dipole moment has again gained in magnitude, and the extracellular field is clearly dominated by this moment, which remains until the hyperpolarization of the cell overshoots the threshold and a relatively strong quadrupole emerges again, although the overall extracellular potential is much smaller at this point.

6 Discussion

We have shown that the extracellular field of a biologically realistic pyramidal cell can be accurately and efficiently calculated at all spatial distances from the cell through a moment expansion of the membrane current distribution. We have formulated the multipole expansion in a form that converges at all points in space, generalizing it from the traditional classical expansion to include test points localized within the sphere of the current distribution.

For the model cell under consideration, we have found that we may divide the extracellular space into three regions. In what we have designated the inner field, which extends from the origin—where we have placed the center of the cell—up to length scales of 0.5 mm, our analysis has shown that the multipole expansion converges slowly, requiring on the order of the first 25 moments to converge to within a few percent of the true extracellular potential. At slightly larger distances, from just outside the boundary between the inner and outer field, $r > 0.5$ mm, the cell displays a strong quadrupole moment that may appreciably contribute to the extracellular potential to distances on the order of 1 cm from the cell. Within this region, the extracellular field may be modeled as originating from an oscillating dipole and quadrupole, while higher moments may be neglected. At length scales $r > 1$ cm, as expected, only the dipole term remains.

In developing this method, we have made several assumptions that should be reconsidered. First, we have taken full advantage of the symmetry displayed by pyramidal cells to reduce the number of terms in the potential expansion. In truth, this is an approximation, as is made clear by Figure 3. It should be noted that for cells without a clear symmetry axis (e.g., Purkinje cells), one would have to account for all $m = -l, \ldots, l$ axial moments. This would likely lead to a large number of terms in the potential expansion, making the procedure impractical. Second, we have treated the extracellular medium as homogeneous, neglecting the effects of other dendrites or axons present within the vicinity of the cell. It would be very difficult, if not impossible, to exactly account for these inhomogeneities; nonetheless, it is an interesting question to ask, for instance, how random defects in the extracellular milieu might modulate the extracellular

field. Third, we have triggered the action potential within the soma and have analyzed the extracellular field generated by the dynamics of the resulting membrane currents. One may also initiate the action potential by distributing the inputs within the synapses and proceed with the analysis we have presented here. Since the method will work for an arbitrary current distribution, only the efficiency of our method should be effected.

As discussed in section 1, the contribution of the action potential is thought to be negligible to EEG measurements. We are now in a better position to test this fundamental assumption. For instance, we may use the method presented here to simulate large populations of biologically realistic spiking neurons and see the effects of orientation and synchrony on the combined extracellular potentials. In particular, we may study the contributions of slower components following the action potential, such as short and longer-lasting afterhyperpolarizations. Unfortunately, due to the complexity of the current dynamics displayed by the model neuron we have used for this study, it is difficult to infer how these slower processes would affect the extracellular fields without fully simulating these fields.

Acknowledgments

We thank Carl Gold for providing us with his NEURON code package. We also acknowledge support from the Swartz Foundation and NSF.

References

Bedard, C., Kroger, H., & Destexthe, A. (2004). Modeling extracellular field potentials and the frequency filtering properties of extracellular space. *Biophysical J.*, *86*, 1829–1842.

Ebersole, J. S. (1997). Defining epileptogenic foci: Past, present, future. *J. Clin. Neurophys.*, *14*, 470–483.

Faber, D. S., & Korn, H. (1989). Electrical field effects: Their relevance in central neural networks. *Physiol. Rev.*, *69*, 821–863.

Gold, C., Henze, D. A., Koch, C., & Buzsaki, G. (2006). On the origin of the extracellular action potential waveform: A modeling study. *Journal of Neurophysiology*, *95*, 3113–3128.

Hines, M. L., & Carnevale, N. T. (1997). The neuron simulation environment. *Neural Comput.*, *9*, 1179–1209.

Hodgkin, A. L., & Huxley A. F. (1952). A quantitative description of membrane current and its application to conduction and excitation in nerve. *J. Physiol.*, *117*, 500–544.

Holt G. R., & Koch C. (1999). Electrical interactions via the extracellular potential near cell bodies. *Journal of Computational Neuroscience*, *6*, 169–184.

Jefferys, J. G. R. (1995). Nonsynaptic modulation of neuronal activity in the brain: Electric current and extracellular ions. *Physiol. Rev.*, *75*, 689–723.

Jirsa, V. K., & Haken, H. (1996). Field theory of electromagnetic brain activity. *Phys. Rev. Lett.*, *77*, 960–963.

Koch, C. (1999). *Biophysics of computation*. New York: Oxford University Press.

Korn, H., & Axelrad, H. (1980). Electrical inhibition of Purkinje cells in the cerebellum of the rat. *Proc. Natl. Acad. Sci.*, *77*, 6244–6247.

Korn, H., & Faber, D. S. (1980). Electrical field effect interactions in the vertebrate brain. *Trends Neurosci.*, *3*, 6–9.

Neves-Petersen, M. T., & Petersen, S. B. (2003). Protein electrostatics: A review of the equations and methods used to model electrostatic equations in biomolecules—applications in biotechnology. *Biotechnol. Annu. Rev.*, *9*, 315–95.

Nunez, P. L., & Srinivasan, R. (2006). *Electric fields of the brain*. New York: Oxford University Press.

Plonsey, R. (1969). *Bioelectric phenomena*. New York: McGraw-Hill.

Price, S. L., Celso, F. L., Treichel, J. A., Goodfellow, J. M., & Umrania, Y. (1993). What base pairings can occur in DNA? A distributed multipole study of the electrostatic interactions between normal and alkylated nucleic acid bases. *J. Chem. Soc.*, *89*, 3407–3417.

Rafat, M., & Popelier, P. L. A. (2005). The electrostatic potential generated by topological atoms. II. Inverse multipole moments. *Journal of Chemical Physics*, *123*, 204103, 1–7.

Robinson, P. A., Rennie, C. J., Rowe, D. L., O'Conner, S. C., & Gordon, E. (2005). Multiscale brain modeling. *Phi. Trans. Roy. Soc. Lon. B*, *360*, 1043–1050.

Robinson, P. A., Rennie, C. J., Wright, J. J., Bahramali, H., Gordon, E., & Rowe, D. L. (2001). Prediction of electroencephalographic spectra from neurophysiology. *Phys. Rev. E.*, *63*, 021903, 1–18

Saraniti, M., Aboud, S., & Eisenberg, R. (2006). The simulation of ionic charge transport in biological ion channels: An introduction to numerical methods. *Reviews in Computational Chemistry*, *22*, 229–293.

Srinivasan, R. (2006). Anatomical constraints on source models for high-resolution EEG and MEG derived from MRI. *Technology in Cancer Research and Treatment*, *5*, 389–399.

Received June 1, 2007; accepted December 28, 2007.